ACS PHYSICAL CHEMISTRY Au
AN OPEN ACCESS JOURNAL OF THE AMERICAN CHEMICAL SOCIETY

pubs.acs.org/physchemau

Perspective

Revisiting the Conformational Isomerism of Dihaloethanes: A Hybrid Computational and Experimental Laboratory for the Undergraduate Curriculum

Blake I. Armstrong, Meg Willans, Emma L. Pearson, Thomas Becker, Mark J. Hackett, and Paolo Raiteri*

Cite This: *ACS Phys. Chem Au* 2023, 3, 157–166

Read Online

ACCESS | Metrics & More | Article Recommendations | Supporting Information

ABSTRACT: The conformational isomerism of disubstituted ethanes is a well-known concept that is part of every chemistry curriculum. Due to the species' simplicity, studying the (free) energy difference between the *gauche* and *anti* isomers has been the testing ground of experimental and computational techniques, such as Raman and IR spectroscopy, quantum chemistry, and atomistic simulations. While students normally receive formal training in spectroscopic techniques during their early undergraduate years, computational methods often receive less attention. In this work, we revisit the conformational isomerism of 1,2-dichloroethane and 1,2-dibromoethane and design a hybrid computational and experimental laboratory for our undergraduate chemistry curriculum with a focus on introducing computational techniques as a complementary research tool to experimentation. We show how commonly available Raman spectrometers and atomistic simulations performed on desktop computers can be combined to study the conformational isomerism of disubstituted ethanes while discussing the advantages and limitations of the different approaches.

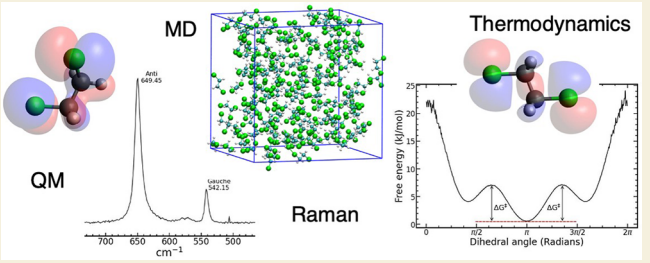

KEYWORDS: *Undergraduate laboratory, Computational chemistry, Raman spectroscopy, dihalo-ethanes, conformational isomerism*

INTRODUCTION

Computational chemistry is an essential research tool, making substantial contributions to both the fields of experimental and theoretical chemistry. For undergraduate chemistry students, the interdisciplinary area of computational chemistry provides an opportunity for authentic learning.[1] Learning outcomes across a curriculum improve when topics are interconnected rather than taught in isolation. In addition, learning outcomes are enhanced when students can link theoretical knowledge with practical applications[2−4] and an inherent application of computational chemistry is the ability to predict and rationalize experimental results.[5] Undergraduate students, however, often receive limited or no exposure to computational techniques.

Training opportunities in computational chemistry may be hindered, at least in part, by either a real or perceived disconnect to undergraduate coursework.[1,6] For example, teaching computational chemistry may require additional computational infrastructure for laboratories and hands-on activities, a different physical or online learning environment, or the need for pre-existing student skills in programming and command line-driven software operation.[1,6] Attempts to tackle these problems have been made by other educators in this field[7] by making use of centralized interfaces, such as WebMO,[8] which aim to simplify the process of performing quantum chemistry calculations to make it more accessible to a wider audience.

In this paper, we describe an integrated physical, organic, and computational chemistry laboratory program developed for fourth-year chemistry students (Honors) which utilizes a readily accessible Raman spectrometer and commodity computers for computational simulations. This laboratory program, structured to be completed over four teaching weeks, provides training in computational chemistry through a familiar and frequently taught undergraduate topic (conformational isomerism) and includes lectures on the theoretical background, data collection, data analysis and report writing. This laboratory has been run for the last three years at our institution as one of the two optional modules of the coursework unit of the Chemistry Honors degree. The unit is timetabled as 4 h a week of workshop/laboratory, but the class is generally small, less than 10 students, which allowed us to tailor the content delivery to the students' needs. The first hour of each workshop is dedicated to introducing the problem and computational techniques that will be used in the laboratory, the remaining 3 h are devoted to the hands-on

Received: October 14, 2022
Revised: December 20, 2022
Accepted: December 22, 2022
Published: January 12, 2023

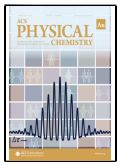

https://doi.org/10.1021/acsphyschemau.2c00055
ACS Phys. Chem Au 2023, 3, 157–166

aspect of the laboratory; setting up the computers, preparing the input and running the simulations. The simulations often take longer than 3 h and the students are asked to leave the simulations running on the virtual machines and collect the results at the next laboratory. The workshop in the fourth week is completely dedicated to collating all the data together and discussing results for the assignment (written report). One further 3 h laboratory is scheduled for collecting the Raman spectra, this can be on any week, depending on the availability of the instrument. The students are encouraged to treat this as a research project and work independently or as a small team. Given our small class sizes one instructor is sufficient to introduce the computational methods in the workshops and one lab technician was used to help out with the Raman measurements.

The choice of conformational isomerism is strategic as it is routinely taught in the undergraduate course, generally early on, and the fundamentals are easily visualized. Indeed, conformational isomerism is traditionally taught "hands-on" with visual aids (e.g., stick and ball models) with the standard example being butane.[9−11] This learning introduces the concept of the Newman projection and the energy plot showing the *anti* isomer being the lowest energy isomer and the two *gauche* isomers being higher in energy due to steric hindrance between the 1 and 4 methyl groups. The concept of steric hindrance as a rationale for the nature of the rotational energy minimum provides a basis for predicting and explaining the structure and reactivity of more complex systems and is our initial link between regular undergraduate coursework and computational chemistry.

Conformational isomerism increases in complexity (and perhaps interest to the engaged student) when one or more of the methyl groups of butane is substituted for an electron-withdrawing or donating group. Students must now consider the role of stereoelectronic effects[12] alongside steric effects and also solvent effects (electrostatics) in intermolecular interactions, with the latter being the focus of this experiment. As such, the study of conformational isomerism in substituted ethanes is instructive for the more advanced chemistry student, as predictions made on purely steric grounds may be incorrect,[13] particularly in the liquid and solid phases. Conformational isomerism of molecules has been extensively studied in the literature, with 1,2-dichloroethane (DCE) arguably being one of the most studied compounds. Indeed, the described laboratory program was inspired, in part, by previous literature using NMR[14] or Raman[15,16] spectroscopy to determine populations of 1,2-dichloroethane (DCE) and 1,2-dibromoethane (DBE). We note the importance of conformational isomerism in 1,2-difluoroethane (DFE) with regards to the *gauche* effect;[17] however, this laboratory program is designed to encourage students to think critically about the effect of intermolecular interactions, in liquid and solvent, on conformation. In addition, DFE is not studied directly in this experiment due to the inherent difficulties associated with handling low boiling liquids.

In this laboratory program students investigate, through computational and experimental methods, the enthalpy difference between the conformational isomers of DCE and DBE. This introduces students to computational techniques and demonstrates how computer simulations and experiments can be used in parallel to tackle the same problem.

Commencing with collecting Raman spectra for liquid samples across a series of temperatures, students are provided with a "hands-on" introduction to the laboratory program, an approach shown to enhance student engagement.[2−4] In addition, the incorporation of Raman spectroscopy provides a means to link this laboratory program back to other facets of a typical undergraduate chemistry curriculum, such as group theory and analytical chemistry. Specifically, the use of Raman spectroscopy enables students to visually observe differences in spectra due to temperature-dependent isomerism, providing increased context for the following computational calculations. Quantum chemical calculations (QM) for gas phase systems and atomistic molecular dynamics (MD) simulations for the liquid systems are then used to tackle the same problem from a different perspective.

Background

In order to successfully undertake this laboratory program, teaching staff must have sufficient understanding of some specific background theory, which the students are then expected to learn during the lab program. The necessary background theory is described below.

When considering disubstituted ethanes, chemistry students are familiar with the energy plot showing the *anti* isomer being the lowest energy isomer and the two *gauche* isomers being higher in energy due to the steric hindrance of the 1,2 substituents. However, it is not often discussed how this energy difference relates to the fraction of molecules in the *anti* and *gauche* isomers and how it can be determined experimentally or predicted using computational methods. This lack of understanding can be attributed to a poor foundation of the underlying statistical mechanics (e.g., the role of the Boltzmann factor) which may be introduced insufficiently during the curriculum.

If we consider the isomerization process as a normal chemical equilibrium reaction, the free energy difference between the *anti* and *gauche* isomers of DCE and DBE can be written in terms of its equilibrium constant $K_{eq} = x_a/x_g$ (eq 1),

$$\Delta G^\circ = -RT \ln\left[\frac{x_a}{x_g}\right] \tag{1}$$

where x_a and x_g are the molar fractions of the *anti* and *gauche* isomers. It is important to note here that there are two equivalent mirror image *gauche* isomers but only one *anti* isomer. In order to account for this, though they have the same energy, a degeneracy factor needs to be included in the calculations of the thermodynamic quantities for this system. To obtain the free energy difference between the *anti* and *gauche* isomers, shown in eq 2, there is a factor of $R \ln 2$ that needs to be added to the entropy

$$\Delta G^\circ = \Delta H^\circ_{ag} - T(\Delta S^\circ_{ag} + R \ln 2) \tag{2}$$

where ΔH°_{ag} and ΔS°_{ag} are the standard enthalpy and entropy differences between the *anti* and one of the two equivalent *gauche* isomers.

In Raman spectroscopy, the total scattering intensity of a given vibrational mode, I_i, which is defined as the integral of the corresponding peak in the spectrum, is directly proportional to the molar fraction (concentration) of the species, x_i, and the scattering cross-section of that particular vibrational mode, σ_i (eq 3)

$$I_i \propto \sigma_i x_i \tag{3}$$

https://doi.org/10.1021/acsphyschemau.2c00055
ACS Phys. Chem Au 2023, 3, 157−166

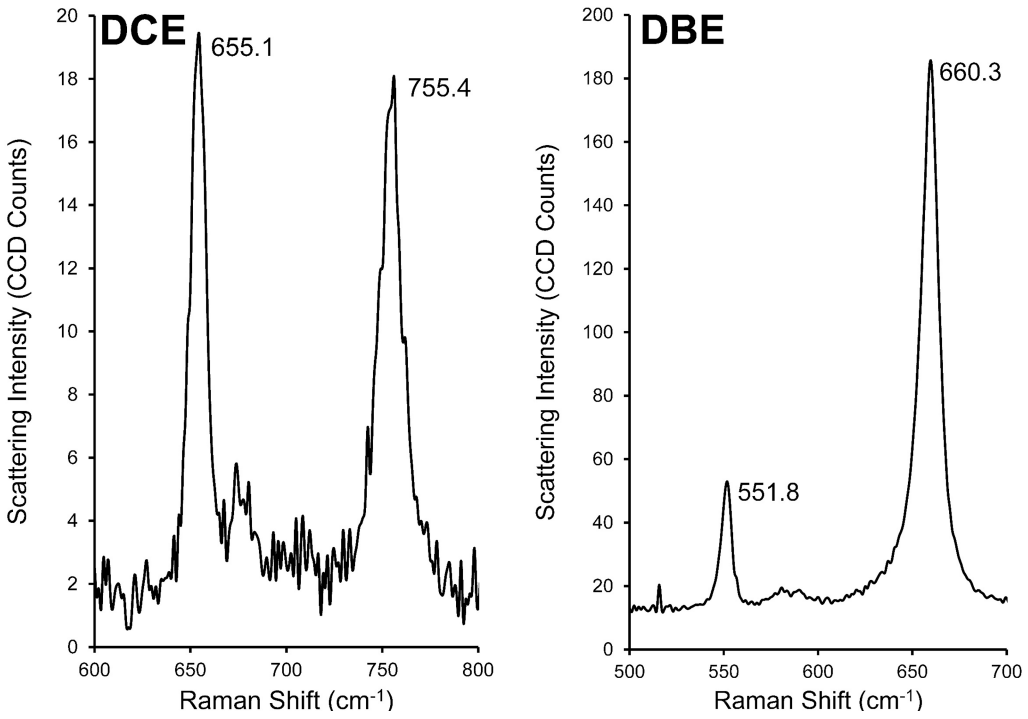

Figure 1. Background corrected spectra of DCE (left) and DBE (right) at 298 K. In each case, the *anti* peak has a higher frequency than the *gauche* peak. The *anti* peak is from the second vibrational mode with a_g symmetry ($\tilde{\nu}_2$) and the *gauche* peak is from the third vibrational mode with *a* symmetry ($\tilde{\nu}_3$).

In the case of molecules that can assume multiple conformations, such as DCE and DBE, each isomer has its own specific set of vibrational frequencies. As such, the Raman spectrum of one of these molecules is a weighted compilation of the individual isomers' Raman spectra, with the weights dependent on the isomers' concentration and the scattering cross sections of the individual modes.[18]

In the case of DCE and DBE, the vibrational frequencies of the symmetric C-X stretching modes (X = Cl,Br) are sufficiently different that it should be possible to use the measured Raman intensities to directly determine the populations of the *anti* and *gauche* isomers, and therefore the free energy difference between the two isomers, as described in eq 4.

$$\ln\left[\frac{I_i^a \sigma_i^g}{I_i^g \sigma_i^a}\right] = \ln\left[\frac{x_a}{x_g}\right] = -\frac{\Delta G^\circ}{RT} \tag{4}$$

In practice, there is no easy way to determine, either experimentally or computationally, what the cross-section of a Raman-active vibrational mode is. For example, Fujiyama and Kakimoto[19] have suggested that a plot of the intensities of a given vibrational mode obtained at different temperatures for the *gauche* isomer vs the corresponding values for the *anti* isomer should display a linear relationship, with the slope corresponding to $-\sigma_g/\sigma_a$. Although this procedure appears to be very simple, it requires correcting the measured Raman intensities for the change in the refractive index of the liquid with temperature, for which there is no easily accessible literature data. For the authors' admission, it worked only for DBE and not for DCE. We have indeed attempted to follow the procedure outlined in ref 19 and could not reproduce their results, which could be due to missing details in their paper. On the other hand, Cappelli et al.[20] performed extensive high level QM calculations to compute the scattering cross-section of selected vibrational modes of DCE in vacuum and various solvents using a continuum solvation model. Reported values for σ_a/σ_g were between 2.8 and 6.7, depending on the vibrational mode and solvent considered. Unfortunately, the scattering cross sections for DCE or DBE were not computed, and, likely, these values would not be directly applicable to Raman spectra acquired for liquid samples.

Despite the limitations to experimentally determining the relative population of the *anti* and *gauche* isomers, it is still possible to determine the enthalpy difference from the measured Raman intensities at different temperatures using eq 5

$$\ln\left[\frac{I_i^a}{I_i^g}\right] = -\frac{\Delta H^\circ}{RT} + C \tag{5}$$

where C is a fitting parameter that contains the standard entropy difference between the *anti* and *gauche* isomers, the ratio of the scattering cross sections, the degeneracy factor, and any multiplicative quantities that connect the Raman intensities to the molar fraction which are generally assumed to be temperature independent. The experimentally determined enthalpy can then be readily compared against computational values obtained in the second part of this experiment using QM and empirical methods. QM simulations for simple systems can nowadays be performed on commodity computers, and they have been shown to produce accurate gas phase energies (see, e.g., refs 21−23), but due to their high computational cost, they cannot be easily used for liquid systems. In fact, in most QM calculations, solvent effects are included indirectly by using implicit solvation models.[24−27] These treat the molecular environment as a dielectric continuum, neglecting any intermolecular interactions, which

https://doi.org/10.1021/acsphyschemau.2c00055
ACS Phys. Chem Au 2023, 3, 157−166

can however play a fundamental role in determining the enthalpy difference between the *anti* and *gauche* isomers of DCE and DBE.[28] On the other hand, atomistic simulations, such as molecular dynamics (MD), allow us to compute ensemble averages of the molecular conformations directly and extract the molar fraction of the two isomers. However, these methods suffer from a lack of accuracy due to the use of empirical formulas to describe the interatomic interactions. Even on commodity computers, empirical MD simulations are fast enough to compute converged ensemble averages of the molecular conformations to determine the molar fractions of the DCE and DBE conformational isomers. Subsequently, by performing a series of calculations at different temperatures, it is then possible to extract the enthalpy difference between the isomers.

In the remainder of this paper, we will describe the techniques used in our laboratory program, analyze the results and briefly discuss the main learning outcomes of this laboratory program.

METHODS

Raman Spectroscopy

All microRaman spectra were recorded with a WITec alpha-300 R confocal Raman spectrophotometer, using 40 coadded scans collected with a 1 s accumulation time. The laser used was a frequency-doubled NdYAG laser with an excitation wavelength of 532 nm. A 20x objective was used with a numerical aperture of 0.4. The samples of DCE and DBE were prepared in sealed glass capillary tubes and analyzed over a temperature range of 283.15 to 333.15 K in increments of 5 K. Triplicate spectra were recorded per temperature interval using a grating of 600 g/mm. The vibrational frequencies used for analysis are shown in Figure 1. The Raman peak areas were integrated using curve fitting within the WITec ProjectFOUR program suite.

Quantum Chemistry

All the quantum chemistry calculations reported in this work have been performed within the Density Functional Theory (DFT) framework with the program ORCA[29] using the B3LYP exchange and correlation functional, the def2-TZVP basis set, and Grimme's D3BJ van der Waals correction.[30,31] The molecules have been optimized in vacuum and with the conductor-like polarizable continuum implicit solvation model (CPCM) as implemented in ORCA.[32] The free energy difference between the isomers was computed from the vibrational frequencies of the optimized molecules using the quasi-harmonic approximation with the vibrational levels populated using the Boltzmann distribution at different temperatures.

The energy barrier for the conformational isomerism was computed using the Climbing Image Nudged Elastic Band (NEB-CI) method[33] to ensure the correct location of the transition state.[34] Given the simple molecular transformation that is required for the conformational isomerism of DCE and DBE, the transition state could be identified by doing a simple scan of the potential energy surface as a function of the Cl−C−C−Cl torsional angle. The NEB is however a more general method that can be applied to cases where it is difficult to guess what the transition state might be, and we have therefore chosen to illustrate the use of this method in this laboratory.

Molecular Dynamics

All MD simulations were performed using the LAMMPS code[35] and the interatomic interactions were described with the GAFF force field,[36]

$$U(r) = \frac{q_i q_j}{r} \tag{6}$$

$$+ 4\epsilon_{ij}\left[\left(\frac{\sigma_{ij}}{r}\right)^{12} - \left(\frac{\sigma_{ij}}{r}\right)^{6}\right] \tag{7}$$

$$+ k_b(b_{ij} - b_0)^2 \tag{8}$$

$$+ k_\theta(\theta_{ijk} - \theta_0)^2 \tag{9}$$

$$+ k_\phi[1 + \cos(n\phi_{ijkl} - \phi_0)] \tag{10}$$

where one can recognize the well know electrostatic (eq 6), van der Waal (eq 7), harmonic stretching (eq 8), bond bending (eq 9) and torsional energy (eq 10) contributions, the force field parameters used in this work are reported in Table 1. The torsional parameters have been slightly modified from the original GAFF force field to better reproduce the observed populations of the *anti* and *gauche* isomers of DCE and DBE at room temperature by Tanabe,[37] and to improve the liquids' dielectric constants.

Table 1. Force field parameters used in the MD simulations. Cc, Hc are the carbon and hydrogen atoms in DCE, and Cb and Hb are the carbon and hydrogen atoms in DBE. The Lorentz−Berthelot combining rules have been used for the van der Waals interactions

Atom type	q_e	ϵ (eV)	σ (Å)
Cc	−0.05810	0.00474	3.39967
Hc	0.13110	0.00068	2.47135
Cl	−0.20410	0.01149	3.47094
Cb	−0.20750	0.00474	3.39967
Hb	0.17710	0.00068	2.47135
Br	−0.14660	0.01821	3.59923
Bond type	**k_b (eV)**		**b_0 (Å)**
Cc−Cc	13.14374		1.535
Cc−Hc	14.56610		1.093
Cc−Cl	12.09866		1.786
Cb−Cb	13.14374		1.535
Cb−Hb	14.56610		1.093
Cb−Br	9.95232		1.966
Angle type	**k_θ (eV)**		**θ_0**
Cc−Cc−Hc	2.01037		110.07
Cc−Cc−Cl	2.50863		110.33
Hc−Cc−Hc	1.69902		109.55
Cl−Cc−Hc	1.76320		105.93
Cb−Cb−Hb	2.01037		110.07
Cb−Cb−Br	2.73330		109.25
Hb−Cb−Hb	1.69902		109.55
Br−Cb−Hb	1.86522		103.04
Torsion type	**k_ϕ (eV)**	**n**	**ϕ_0**
Hc−Cc−Cc−Hc	0.00675	3	0
Cl−Cc−Cc−Hc	0.01084	1	0
Cl−Cc−Cc−Cl	0.003	1	180
Hb−Cb−Cb−Hb	0.00675	3	0
Br−Cb−Cb−Hb	0.02385	1	0
Br−Cb−Cb−Br	0.04	1	0

Systems of liquid DCE and DBE were modeled using a cubic 3D periodic cell with a side length of 50 Å consisting of 1150 and 850 molecules, respectively. Each system was equilibrated in the NPT ensemble at the desired temperature until the density converged, followed by production runs in the NVT ensemble using a 1 fs time step for both. The target temperatures were maintained using the

https://doi.org/10.1021/acsphyschemau.2c00055
ACS Phys. Chem Au 2023, 3, 157−166

Bussi-Donadio-Parrinello velocity-rescaling thermostat[38] with a relaxation time of 0.1 ps. Simulation runs at each temperature were performed for 5 ns with three replicates to ensure sufficient statistics for analysis. Systems of gaseous DCE and DBE were modeled using a cubic 3D nonperiodic cell consisting of a single molecule. Each system was run in the NVT ensemble using a 1 fs time step with the same thermostat and relaxation time as in the liquid systems. Simulation runs at each temperature were performed for 50 ns with five replicates to ensure sufficient statistics for analysis.

RESULTS

Although the first part of the laboratory experiment might be to collect Raman spectra, followed by the computational work, it is more instructive to analyze the results in reverse. First, we discuss the gas phase QM calculations which can be readily interpreted using simple steric arguments. We then analyze the empirical force field simulations, which require the introduction of intermolecular forces, before finally comparing the computational results with the experimental measurements to validate the methods used.

Quantum Chemistry

Given the simplicity of the system, the energy difference between the *anti* and *gauche* isomers can been computed with different levels of theory, including MP2 and coupled clusters (Table 2). However, the substantial increase in computational cost does not significantly change the relative stability of the isomers and the B3LYP def2-TZVP with Grimees' D3BJ van der Waals correction[30,31] is deemed sufficient for the purpose of introducing computational chemistry to the undergraduate students. Indeed, it becomes prohibitively expensive to compute the vibrational modes and the Raman spectra using more accurate methods such as MP2/MP3 or Domain-based Local Pair Natural Orbital Coupled Cluster with extrapolation to complete basis method.

Table 2. Energy of the *gauche* Conformer and of the Transition State Relative to That of the *anti* Conformer Computed in Vacuum Using Different Level of Theories[a]

	ΔE_g(kJ/mol)		ΔE_{TS}(kJ/mol)	
Method	DCE	DBE	DCE	DBE
RI BP86 def2-TZVP def2/J	6.4	9.9	17.9	20.6
B3LYP def2-TZVP	6.8	10.3	18.2	20.6
B3LYP RIJCOSX def2-TZVP	6.8	10.3	18.2	20.6
wB97X def2-TZVP	4.5	6.0	18.0	19.4
B3LYP D3BJ def2-TZVP	**5.7**	**8.7**	**18.4**	**20.6**
RIJK RI-B2PLYP D3BJ def2-TZVP	5.7	8.1	19.3	21.2
RIJCOSX RI-B2PLYP D3BJ def2-TZVP	5.8	8.1	19.3	21.2
RIJK RI-PWPB95 D3BJ def2-TZVP	5.4	7.4	18.8	20.7
RI-MP2 RIJCOSX aug-cc-pVTZ	5.5	7.1	20.1	21.9
SCS-MP3 cc-pVTZ	6.2	8.1	20.0	21.8
DLPNO-MP2 DEF2-QZVPP	5.3	7.1	20.3	21.9
DLPNO−CCSD DEF2-QZVPP	5.8	7.7	18.9	20.3
DLPNO−CCSD(T) EXTRAPOLATE(3)	5.8	6.9	18.2	19.5

[a]The energies were computed using the optimized geometries using the recommended method for this laboratory B3LYP D3BJ def2-TZVP, in bold font. The table starts from the quickest method and finishes with arguably the most accurate method.

The thermochemical data for the conformational isomerism of DCE and DBE obtained from the frequency calculations using the B3LYP def2-TZVP D3BJ level of theory are reported in Table 3. As expected, based on previous literature, the *gauche* isomer is always unfavored compared to the *anti* one, with the energy difference for DBE greater than that of DCE attributable to the larger size of Br and the decrease in *gauche* effect down the periodic table.[39] This trend is maintained in the liquid phase. However, it is interesting to note that approximating solvent effects with a simple continuum model significantly reduces the energy difference between the isomers. The *anti* to *gauche* isomerization activation energy (E_a) is also consistent with the notion that Br is larger than Cl. However, the predicted rotation barrier with the PCM implicit solvation model shows a much smaller change in the energy difference between the isomers. The presence of a dielectric medium has a larger effect on the more polar *gauche* isomer than on the *anti* isomer or the transition state.

Table 3. Enthalpy, Entropy, and Free Energy (at 298.15 K) of the *gauche* Isomers Relative to the *anti* Isomer for DBE/DCE in the Gas and Liquid Phases as Predicted from QM Calculations[a]

	DCE		DBE	
	Gas	Liquid	Gas	Liquid
ΔH(kJ/mol)	+5.0	+0.1	+7.9	+4.2
ΔS(J/mol/K)	−1.2	−1.6	−2.9	−3.2
ΔG(kJ/mol)	+5.6	+0.6	+8.7	+5.2
E_a(kJ/mol)	+18.5	+17.7	+20.7	+20.0

[a]The activation energy, free energy difference, and molar fraction were computed at 298 K. The quasiharmonic approximation was used to populate the vibrational modes according to the Boltzmann distribution at that temperature. The liquid phase was simulated using an implicit solvent model (PCM), see text for more details. At 298 K the term $RT \ln 2$ is equal to 1.7 kJ/mol.

QM calculations are also used to routinely compute the vibrational modes of molecules, which in turn can be used to predict the Raman spectrum of a compound. Although it is well-known that the frequencies computed from QM methods have a systematic shift from the experimentally measured ones, they are still useful to guide experiments in assigning the measured peaks. In particular, ORCA has the built-in capability of computing the Raman spectrum of a given compound, which provides useful information about which frequencies are Raman active (i.e., are observed in the experimental spectra). Presented in Table 4 are the QM vibrational frequencies for the normal modes of the symmetric C-X stretching modes,

Table 4. Calculated Vibrational Frequencies Obtained from our DFT Calculations for the C-X Stretching Mode (X = Cl,Br) of the *anti* and *gauche* Isomers for the Gas/Liquid Phases[a]

	DCE		DBE	
	anti ($\tilde{\nu}_2$)	*gauche* ($\tilde{\nu}_3$)	*anti* ($\tilde{\nu}_2$)	*gauche* ($\tilde{\nu}_3$)
Liquid exp. (this work)	755	655	660	552
Vacuum calculations	748	653	654	547
Liquid calculations	727	629	640	532
Fujiyama et al.[19]	754	654	660	551
Tanabe[37,40]	754	669	660	550

[a]In ascending order, $\tilde{\nu}_2$ is the second vibrational mode with a_g symmetry and $\tilde{\nu}_3$ is the third vibrational mode with a symmetry. The vibrational frequencies for the liquid have been estimated using an implicit solvent model (see text). The experimental frequencies measured in this work for the liquids at 298 K agree well with literature values.

https://doi.org/10.1021/acsphyschemau.2c00055
ACS Phys. Chem Au 2023, 3, 157−166

which will be used in the spectroscopy section of this laboratory to compute the enthalpy difference between the *anti* and *gauche* isomers (Figure 1). A very close agreement is observed between the calculated vibrational frequencies in the gas/liquid phase and the experiments, which is not surprising given the simplicity of the molecules at hand.

Molecular Dynamics

One of the most used outputs of an MD simulation is the time evolution of the atoms' positions, usually referred to as a *trajectory*. MD trajectories can then be readily analyzed to compute any quantities and their time averages, which are then assumed to correspond to thermodynamic (ensemble) averages at the simulation temperature (i.e., they can be directly compared with experimental observation). In the case of MD simulations of DCE and DBE, both in the gas and liquid phases, we can use the trajectory to compute the probability that a given molecule displays a given value for the X−C−C−X torsional angle. This is done by computing the torsional angle for each molecule of the system in each frame of the recorded trajectory and then binning them into a histogram. Normalizing the histogram then gives the probability of observing any given torsional angle (Figure 2),

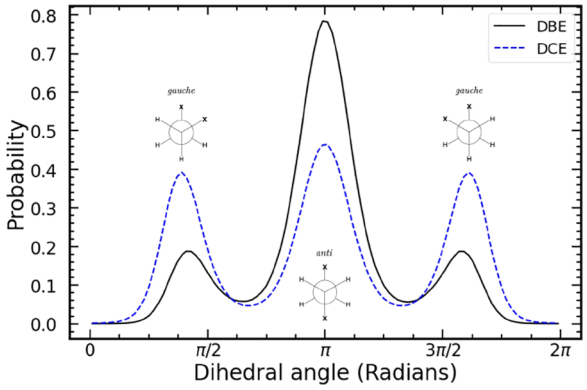

Figure 2. Line plot representation of the normalized histogram of the torsional angle distribution of liquid DBE and DCE at 298 K with the corresponding Newman projections of the isomers at each peak.

which can then be used to compute the fraction of molecules in the two isomers by simple numerical integration (eq 11)

$$x_a = \int_{\theta_0}^{\theta_1} P(\theta)\, \mathrm{d}\theta \tag{11}$$

where $P(\theta)$ is the normalized probability, θ_0 and θ_1 are the boundaries of the region that can be assigned the *anti* isomer, which we chose as the position of the two local minima surrounding the central peak of the probability distribution shown in Figure 2. The molar fraction of the *gauche* isomer can then be readily calculated as $1 - x_a$ or by integrating the rest of the probability distribution.

Equation 1 can then be used to calculate the free energy difference between the isomers at each temperature. The enthalpy and entropy differences between the isomers, which are assumed to be temperature independent, are then readily obtained from a linear fit of the free energy values as a function of temperature. Figure 3 shows the resulting plot from following this procedure for DCE and DBE both in the gas and liquid phases, with the calculated values for the enthalpy and entropy of conformational isomerism presented in Table 5.

The free energy barrier for the conformational isomerism can also be readily computed by transforming the normalized probability into a free energy profile (eq 12)

$$\Delta G(\theta) = -RT \ln P(\theta) \tag{12}$$

and calculating the difference between the free energy minimum of the *anti* isomer and the averaged heights of the adjacent maxima (Figure 4). Although the variations are small, they are statistically significant and clearly show that the activation free energy depends on the temperature, except for DBE in the gas phase. Therefore, in order to predict the rate of conformational isomerism, one would need to go beyond the Arrhenius equation and use Transition State Theory and the Eyring equation to extract the enthalpy and entropy of activation from the free energy of activation (eq 13),

$$\Delta G^{\ddagger} = \Delta H^{\ddagger} - T\Delta S^{\ddagger} \tag{13}$$

which are presented in Table 5.

Raman Spectroscopy

A series of Raman spectra were collected for liquid DCE and DBE at different temperatures. The temperature was initially set to the lowest value of the chosen range and incrementally increased after each spectrum was collected. The *anti* /*gauche* intensity ratios from the Raman spectra were calculated by integrating the area under the labeled peaks shown in Figure 1, and plotted against the temperature Figure 5 (the spectra

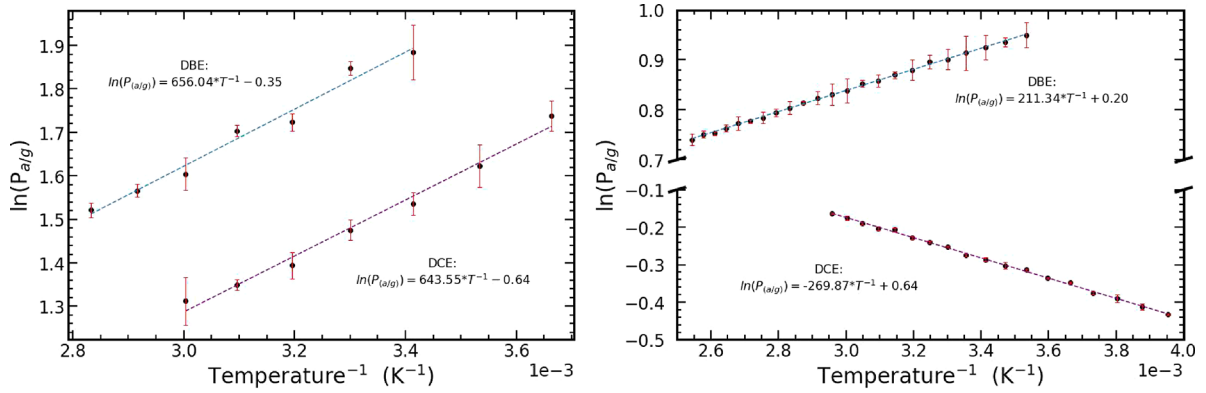

Figure 3. Variation of the *anti* /*gauche* ratio of gaseous (left) and liquid (right) DBE and DCE with temperature. The error bars represent 95% confidence intervals.

https://doi.org/10.1021/acsphyschemau.2c00055
ACS Phys. Chem Au 2023, 3, 157−166

Table 5. Enthalpy and Entropy of the *gauche* Isomers Relative to That of the *anti* Isomer for DBE/DCE in the Gas and Liquid Phases as Predicted by the Empirical Force Field Simulations[a]

	DCE		DBE	
	Gas	Liquid	Gas	Liquid
ΔH(kJ/mol)	5.4 ± 0.3	−2.24 ± 0.02	5.5 ± 0.4	1.76 ± 0.01
ΔS(J/mol/K)	5.3 ± 0.9	−5.28 ± 0.05	2.9 ± 1.1	−1.70 ± 0.03
$\Delta H^{\ddagger}$(kJ/mol)	7.5 ± 0.2	4.80 ± 0.02	7.2 ± 0.3	5.69 ± 0.02
$\Delta S^{\ddagger}$(J/mol/K)	−2.2 ± 0.8	3.05 ± 0.06	−0.0 ± 1.1	2.74 ± 0.05

[a]The enthalpy ($\Delta H^{\ddagger}$) and entropy ($\Delta S^{\ddagger}$) of the conformational isomerism barrier for the *anti* to *gauche* transition is also reported. uncertainties are presented as 95% confidence intervals.

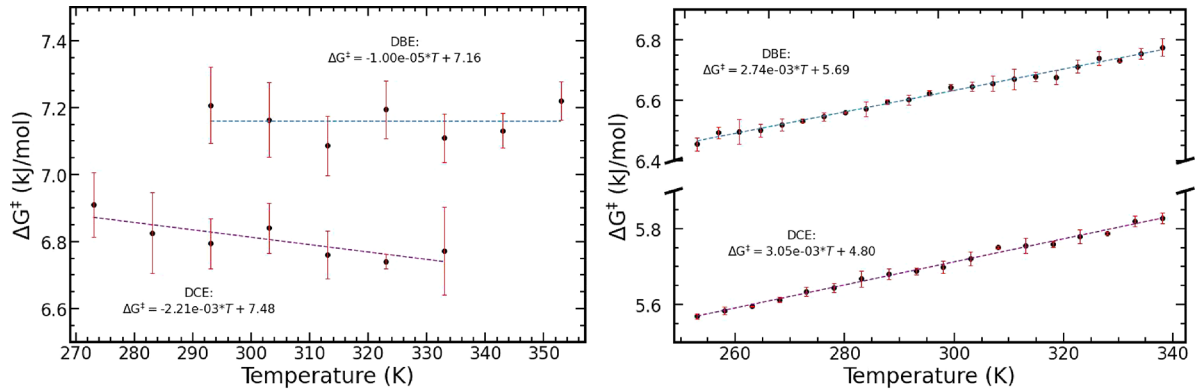

Figure 4. Variation of the conformational isomerism free energy barrier of gaseous (left) and liquid (right) DBE and DCE with temperature. The error bars represent 95% confidence intervals.

collected at all temperatures are shown in Figure S1 in the Supporting Information).

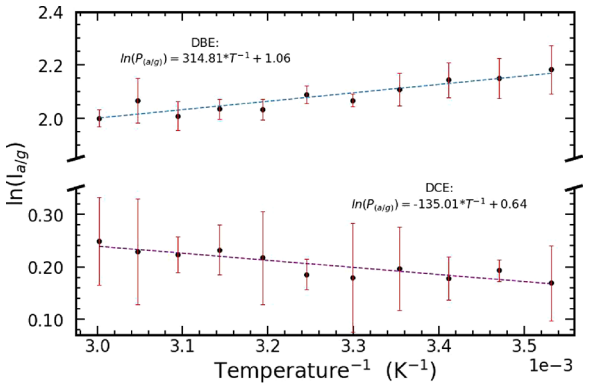

Figure 5. Variation of the *anti* /*gauche* ratio of both liquid DBE and DCE with temperature, obtained from Raman spectroscopy (532 nm laser excitation).

The enthalpy difference between the *gauche* and *anti* isomers can then be readily obtained using eq 5. The calculated enthalpies were −1.12 ± 0.20 and 2.62 ± 0.36 kJ/mol for DCE and DBE, respectively.

DISCUSSION

The techniques used in this work are highly accessible, with a readily available Raman spectrometer used for the spectroscopy aspect and commodity computers used for the QM/MD simulations (or a cloud computing service). Even so, the calculated enthalpies of conformational isomerism are in excellent agreement with published literature values[37,41−43] (Table 6). The values obtained from MD simulations of the liquid phases show the worst agreement with experimental values and the more accurate QM calculations. This disagreement is likely attributed to the GAFF force field parameters not having been properly optimized for these systems. Regardless of the technique used, it is clear how solvent effects contribute to the stabilization of the *gauche* isomer, which, in the case of DCE, is the most abundant in the liquid

Table 6. Summary of the Enthalpy of Conformational Isomerism from *anti* to *gauche* for DCE/DBE Obtained from the Spectroscopic Experiments Performed in This Work Compared with Literature Values

	DCE		DBE	
	Gas	Liquid	Gas	Liquid
DFT	5.0	0.1	7.9	3.3
MD	5.35 ± 0.28	−2.24 ± 0.02	5.45 ± 0.36	1.76 ± 0.01
Raman		−1.12		2.62
Lee et al.[41]		0.0		3.7
Tanabe[37]	4.6 ± 0.3	−0.04 ± 0.4	7.0 ± 0.5	3.1 ± 0.5
Wiberg et al.[42]	4.2−4.8			
Sreeruttun et al.[43]	6.1−8.2		6.7−11.3	

https://doi.org/10.1021/acsphyschemau.2c00055
ACS Phys. Chem Au 2023, 3, 157−166

phase at ambient conditions (Table 7). The stabilization of the *gauche* isomer in the liquid phase is well documented in the

Table 7. Molar Fraction of the *gauche* Isomer at 298 K as Predicted by the QM and MD Simulations Performed in This Work and from Literature

	DCE		DBE	
	Gas	Liquid	Gas	Liquid
DFT	0.18	0.61	0.05	0.20
MD	0.18	0.57	0.14	0.29
Tanabe[37]	0.23	0.65	0.10	0.36

literature. For example, the computational work by Wiberg et al.[42] showed how the *gauche* isomer is progressively stabilized in solvents with larger dielectric solvents (i.e., more polar solvents). It was predicted that the crossover in the stability of the *anti* and *gauche* isomers of DCE should occur in solvents that have a dielectric constant in the range 7 to 20, which bracket the dielectric constant of the liquid (ε_r = 10.3) and is consistent with both the experiments and simulations performed in this laboratory experiment. A similar stabilization of the *gauche* isomer is observed for DBE. However, due to the larger size of Br atoms, the crossover in stability between the *anti* and *gauche* isomers is not observed in the liquid phase (ε_r = 4.75).

It is instructive to discuss the stabilization effect of the *gauche* isomer observed in polar solvents in terms of the electrostatic intermolecular interactions. While the *anti* isomer has no permanent dipole moment, the *gauche* isomer does (Table 8), which can favorably interact with the dipoles in the

Table 8. Dipole Moment of the *gauche* Isomer of DCE and DBE Obtained from our QM Calculations in the Gas and Liquid Phases (PCM)

DCE		DBE	
Gas	Liquid	Gas	Liquid
2.72	3.85	2.65	3.72

solvent molecules. Therefore, the energy penalty (steric hindrance) of the *gauche* isomer is offset by the favorable (negative) electrostatic interaction with the solvent. In the case of liquid DCE/DBE (a mixture of the *anti* and *gauche* isomers), one can interpret this as a self-stabilization effect between the *gauche* isomers. With an increasing abundance of *gauche* isomers in the liquid, the total energy cost of having the high energy isomer and the dipole−dipole interaction energy increase. Due to the low energy barrier for the interconversion between isomers, the system is in a dynamic equilibrium. The computationally predicted dipole moment of the DCE and DBE *gauche* isomers are very similar, consistent with the observation that the solvent-induced stabilization of the isomers is of the order of 4 kJ/mol for both species. However, because of the larger steric hindrance in DBE, the fraction of molecules in the *gauche* isomer remains smaller than that for DCE (Table 7).

The computer simulations also gave us access to the rotational barriers between the isomers, which can be used to discuss the kinetics of the conformational isomerism in terms of the energy required to reach the transition state (Tables 3 and 5). From a qualitative point of view, results from the QM and MD simulation show the same trend, with higher activation energy for DBE than for DCE. Consistently, they also predict that the conformational isomerism activation energy will be lower in the liquid phase.

However, to make a quantitative comparison between the results obtained from QM and MD, one has to consider the intrinsic differences between the two methodologies. The transition state energy obtained from the QM calculations using the CI-NEB method is effectively the rotation barrier at 0 K, where all entropy contributions are neglected. On the other hand, MD allows us to compute the free energy barrier ($\Delta G^{\ddagger}$) for the conformational isomerism at different temperatures, which can then be used in conjunction with the transition state theory to extract the enthalpy and entropy of the transition state, ($\Delta H^{\ddagger}$ and $\Delta S^{\ddagger}$). Although this might be beyond the scope of most undergraduate laboratories, we feel it provided an important discussion point about the common assumption that the activation energy used in the Arrhenius equation is temperature-independent. The use of more sophisticated theories, such as Transition State Theory and the Eyring equation, to interpret the kinetics of a reaction should be considered. Of course, one should also not forget that no computational method is 100% accurate. All the approximations made in the description of the intermolecular interactions and the statistical errors in MD may lead to significant errors in the predicted quantities. Nonetheless, computational methods can provide useful information about the expected trends observed in the experiments.

CONCLUSION

Undergraduates deserve an understanding of the techniques used in computational chemistry, not only so they can effectively utilize them but also to understand and question their usefulness and applicability. However, computational tools are limited at the undergraduate and postgraduate levels, with students often gaining little or no exposure to them. As such, described is an integrated computational and instrumental experiment designed to both (a) challenge and improve students' understanding of simple concepts learned in undergraduate courses, and (b) develop an understanding of the intricate interplay between computational and experimental techniques.

The computer simulations performed in this work provide a useful example of the applicability of MD and QM calculations to predict thermodynamic properties as a complementary tool for experiments. The importance of accurate force field parametrization is highlighted by comparing the computational results with the experiments. At a fundamental level, the quantitative analysis and calculation of thermodynamic properties are investigated, with the effects of intermolecular forces and solvent effects on these properties considered in detail.

This paper described a self-contained experiment that can be readily included in most chemistry degrees. It requires using a Raman spectrometer (albeit with a temperature stage) and commodity (or cloud) computing facilities. This laboratory can also be the foundation for more comprehensive experiments where different experimental and computational techniques can be included to further develop the student's knowledge in specific fields. For example, extensions on this work can include, but are not limited to

- the use of IR and/or NMR spectroscopy
- the collection of gas phase spectra alongside liquid spectra, which require longer measurement times

https://doi.org/10.1021/acsphyschemau.2c00055
ACS Phys. Chem Au 2023, 3, 157−166

- analysis of the molecular orbitals in the *anti*, *gauche*, and transition states.
- optimization of the force field parameters for the MD simulations to better reproduce the experiments
- the use of advanced sampling techniques (metadynamics, umbrella sampling, etc.) to compute the free energy of conformational isomerism as a function of the torsional angle
- exploration of different computational methods
- experiments and/or simulations with other 1,2 dihaloethane molecules, e.g., FCH_2CH_2F or $ClCH_2CH_2Br$.

From an educational point of view, the last point is particularly interesting as the students can be asked to make a prediction based on the results for DCE and DBE, which can then be verified "hands-on" by performing the simulations and the experiments in the laboratory.

■ ASSOCIATED CONTENT

Supporting Information

The Supporting Information is available free of charge at https://pubs.acs.org/doi/10.1021/acsphyschemau.2c00055.

Optimized geometries of the molecules at the B3LYP D3BJ level of theory, Raman spectra of the liquids at all temperatures; lab manual, instructor notes, and assessment guidelines (PDF)

■ AUTHOR INFORMATION

Corresponding Author

Paolo Raiteri − *School of Molecular and Life Sciences and Curtin Institute for Computation, Curtin University, Perth, Western Australia 6845, Australia;* orcid.org/0000-0003-0692-0505; Email: p.raiteri@curtin.edu.au

Authors

Blake I. Armstrong − *School of Molecular and Life Sciences and Curtin Institute for Computation, Curtin University, Perth, Western Australia 6845, Australia*

Meg Willans − *School of Molecular and Life Sciences and Curtin University, Perth, Western Australia 6845, Australia*

Emma L. Pearson − *School of Molecular and Life Sciences and Curtin University, Perth, Western Australia 6845, Australia*

Thomas Becker − *School of Molecular and Life Sciences and Curtin University, Perth, Western Australia 6845, Australia*

Mark J. Hackett − *School of Molecular and Life Sciences and Curtin University, Perth, Western Australia 6845, Australia*

Complete contact information is available at: https://pubs.acs.org/10.1021/acsphyschemau.2c00055

Author Contributions

CRediT: **Blake Armstrong** data curation (equal), investigation (equal), methodology (equal), writing-original draft (equal), writing-review & editing (equal); **Meg Willans** data curation (equal), investigation (equal), methodology (equal), writing-review & editing (equal); **Emma Louise Pearson** data curation, investigation, writing-review & editing; **Thomas Becker** data curation, investigation (equal), writing-review & editing; **Mark J. Hackett** conceptualization (equal), data curation, investigation, methodology (equal), writing-review & editing; **Paolo Raiteri** conceptualization (equal), data curation (equal), investigation, methodology (equal), writing-review & editing (equal).

Notes

The authors declare no competing financial interest.

All the input files used for the simulations done in this work are available on zenodo.org: DOI: 10.5281/zenodo.7460370.

■ ACKNOWLEDGMENTS

The authors thank the Pawsey Supercomputing Centre for the provision of the cloud computing resources that have been used for the computational work. BA thanks the Australian Research Council for his Ph.D. scholarship as part of the grant FL180100087. MJH and MW acknowledge support from the Australian Research Council through a Future Fellowship (FT190100017).

■ REFERENCES

(1) Tuvi-Arad, I. Computational Chemistry in the undergraduate classroom − pedagogical considerations and teaching challenges. *Isr. J. Chem.* **2022**, *62*, No. e2021000.

(2) Cooper, M. M.; Stowe, R. L. Chemistry Education Research—From Personal Empiricism to Evidence, Theory, and Informed Practice. *Chem. Rev.* **2018**, *118*, 6053−6087.

(3) Seery, M. K. Establishing the Laboratory as the Place to Learn How to Do Chemistry. *J. Chem. Educ.* **2020**, *97*, 1511−1514.

(4) Bretz, S. L. Evidence for the Importance of Laboratory Courses. *J. Chem. Educ.* **2019**, *96*, 193−195.

(5) Esselman, B. J.; Hill, N. J. Integrating computational chemistry into an organic chemistry laboratory curriculum using WebMO. *ACS Symp. Ser.* **2019**, *1312*, 139−162.

(6) Johnson, L. E.; Engel, T. Integrating computational chemistry into the physical chemistry curriculum. *J. Chem. Educ.* **2011**, *88*, 569−573.

(7) Adams, W.; Sonntag, M. D. An Upper Level Laboratory Exercise to Explore Computational Predictions of Regiochemistry in Electrophilic Aromatic Substitution. *J. Chem. Educ.* **2022**, *99*, 957−963.

(8) Polik, W. F.; Schmidt, J. R. WebMO: Web-based computational chemistry calculations in education and research. *Wiley Interdiscip. Rev.: Comput. Mol. Sci.* **2022**, *12*, No. e1554.

(9) Kingsbury, C. A. Conformations of substituted ethanes. *J. Chem. Educ.* **1979**, *56*, 431−437.

(10) Blauch, D. N.; Carroll, F. A. 3D Printers Can Provide an Added Dimension for Teaching Structure−Energy Relationships. *J. Chem. Educ.* **2014**, *91*, 1254−1256.

(11) Esselman, B. J.; Hill, N. J. Integration of Computational Chemistry into the Undergraduate Organic Chemistry Laboratory Curriculum. *J. Chem. Educ.* **2016**, *93*, 932−936.

(12) Alabugin, I. V.; Zeidan, T. A. Stereoelectronic Effects and General Trends in Hyperconjugative Acceptor Ability of σ Bonds. *J. Am. Chem. Soc.* **2002**, *124*, 3175−3185.

(13) Pophristic, V.; Goodman, L. Hyperconjugation not steric repulsion leads to the staggered structure of ethane. *Nature* **2001**, *411*, 565−568.

(14) Erickson, L. E.; Morris, K. F. The Energy Profile for Rotation about the C-C Bond in Substituted Ethanes: A Multi-Part Experimental Computational Project for the Physical Chemistry Laboratory. *J. Chem. Educ.* **1998**, *75*, 900−906.

(15) Wladkowski, B. D.; Broadwater, S. J. Determination of the Rotameric Stability of 1,2-Dihaloethanes Using Infrared Spectroscopy. A Combined Experimental and Computational Project for the Physical Chemistry Laboratory. *J. Chem. Educ.* **2002**, *79*, 230−234.

(16) Young, M. D.; Borjemscaia, N. C.; Wladkowski, B. D. Quantitative Determination of the Rotameric Energy Differences of 1,2-Dihaloethanes Using Raman Spectroscopy - an Experimental Project for the PhysicalChemistry Laboratory. *J. Chem. Educ.* **2005**, *82*, 912−915.

(17) Port, V. C.; Cormanich, R. A. There and back again: the role of hyperconjugation in the fluorine gauche effect. *Phys. Chem. Chem. Phys.* **2021**, *23*, 17329−17337.

(18) Dare-Edwards, M. P.; Gardiner, D. J.; Walker, N. A. Raman intensity measurements for determining conformer populations as a function of pressure. *Nature* **1985**, *316*, 614−616.
(19) Fujiyama, T.; Kakimoto, M. Rotational Isomerism and Intermolecular Interaction in the Liquid Phase. *Bull. Chem. Soc. Jpn.* **1976**, *49*, 2346−2350.
(20) Cappelli, C.; Corni, S.; Tomasi, J. Solvent Effects on trans/gauche Conformational Equilibria of Substituted Chloroethanes: a Polarizable Continuum Model Study. *J. Phys. Chem. A* **2001**, *105*, 10807−10815.
(21) Goerigk, L.; Grimme, S. A thorough benchmark of density functional methods for general main group thermochemistry, kinetics, and noncovalent interactions. *Phys. Chem. Chem. Phys.* **2011**, *13*, 6670−6688.
(22) Goerigk, L.; Hansen, A.; Bauer, C.; Ehrlich, S.; Najibi, A.; Grimme, S. A look at the density functional theory zoo with the advanced GMTKN55 database for general main group thermochemistry, kinetics and noncovalent interactions. *Phys. Chem. Chem. Phys.* **2017**, *19*, 32184−32215.
(23) Ho, J.; Coote, M. L. First-principles prediction of acidities in the gas and solution phase. *WIREs Comput. Mol. Sci.* **2011**, *1*, 649−660.
(24) Cossi, M.; Barone, V.; Cammi, R.; Tomasi, J. Ab initio study of solvated molecules: a new implementation of the polarizable continuum model. *Chem. Phys. Lett.* **1996**, *255*, 327−335.
(25) Cancès, E.; Mennucci, B.; Tomasi, J. A new integral equation formalism for the polarizable continuum model: Theoretical background and applications to isotropic and anisotropic dielectrics. *J. Chem. Phys.* **1997**, *107*, 3032−3041.
(26) Lee, J. Y.; Yoshida, N.; Hirata, F. Conformational equilibrium of 1,2-dichloroethane in water: comparison of PCM and RISM-SCF methods. *J. Phys. Chem. B* **2006**, *110*, 16018−16025.
(27) Marenich, A. V.; Cramer, C. J.; Truhlar, D. G. Universal Solvation Model Based on Solute Electron Density and on a Continuum Model of the Solvent Defined by the Bulk Dielectric Constant and Atomic Surface Tensions. *J. Phys. Chem. B* **2009**, *113*, 6378−6396.
(28) Boereboom, J. M.; Fleurat-Lessard, P.; Bulo, R. E. Explicit Solvation Matters: Performance of QM/MM Solvation Models in Nucleophilic Addition. *J. Chem. Theory Comput.* **2018**, *14*, 1841−1852.
(29) Neese, F.; Wennmohs, F.; Becker, U.; Riplinger, C. The ORCA quantum chemistry program package. *J. Chem. Phys.* **2020**, *152*, No. e224108.
(30) Grimme, S.; Antony, J.; Ehrlich, S.; Krieg, H. A consistent and accurate ab initio parametrization of density functional dispersion correction (DFT-D) for the 94 elements H-Pu. *J. Chem. Phys.* **2010**, *132*, No. e154104.
(31) Grimme, S.; Ehrlich, S.; Goerigk, L. Effect of the damping function in dispersion corrected density functional theory. *J. Comput. Chem.* **2011**, *32*, 1456−1465.
(32) Barone, V.; Cossi, M. Quantum calculation of molecular energies and energy gradients in solution by a conductor solvent model. *J. Phys. Chem. A* **1998**, *102*, 1995−2001.
(33) Henkelman, G.; Uberuaga, B. P.; Jónsson, H. A climbing image nudged elastic band method for finding saddle points and minimum energy paths. *J. Chem. Phys.* **2000**, *113*, 9901−9904.
(34) Henkelman, G.; Uberuaga, B. P.; Jónsson, H. A climbing image nudged elastic band method for finding saddle points and minimum energy paths. *J. Chem. Phys.* **2000**, *113*, 9901−9904.
(35) Thompson, A. P.; Aktulga, H. M.; Berger, R.; Bolintineanu, D. S.; Brown, W. M.; Crozier, P. S.; in 't Veld, P. J.; Kohlmeyer, A.; Moore, S. G.; Nguyen, T. D.; Shan, R.; Stevens, M. J.; Tranchida, J.; Trott, C.; Plimpton, S. J. LAMMPS - a flexible simulation tool for particle-based materials modeling at the atomic, meso, and continuum scales. *Comput. Phys. Commun.* **2022**, *271*, No. e108171.
(36) Sprenger, K. G.; Jaeger, V. W.; Pfaendtner, J. The General AMBER Force Field (GAFF) Can Accurately Predict Thermodynamic and Transport Properties of Many Ionic Liquids. *J. Phys. Chem. B* **2015**, *119*, 5882−5895.
(37) Tanabe, K. Calculation of infrared band intensities and determination of energy differences of rotational isomers of 1,2-dichloro-, 1,2-dibromo- and 1-chloro-2-bromoethane. *Spectrochim. Acta A-M* **1972**, *28*, 407−424.
(38) Bussi, G.; Donadio, D.; Parrinello, M. Canonical sampling through velocity rescaling. *J. Chem. Phys.* **2007**, *126*, No. e014101.
(39) Rodrigues Silva, D.; de Azevedo Santos, L.; Hamlin, T. A.; Fonseca Guerra, C.; Freitas, M. P.; Bickelhaupt, F. M. The Gauche Effect in XCH2CH2X Revisited. *ChemPhysChem* **2021**, *22*, 641−648.
(40) Tanabe, K.; Hiraishi, J.; Tamura, T. Vibrational frequencies and infrared absorption intensities of 1,2-dibromoethane. *J. Mol. Struct.* **1976**, *33*, 19−37.
(41) Lee, I.-C.; Hamaguchi, H.-o.; Shigeto, S. The trans/gauche conformational equilibrium and associated thermodynamic parameters of liquid 1,2-dibromoethane as studied by infrared electroabsorption spectroscopy. *Chem. Phys. Lett.* **2008**, *466*, 144−147.
(42) Wiberg, K. B.; Keith, T. A.; Frisch, M. J.; Murcko, M. Solvent Effects on 1,2-Dihaloethane Gauche/Trans Ratios. *J. Phys. Chem.* **1995**, *99*, 9072−9079.
(43) Sreeruttun, R. K.; Ramasami, P. Conformational behaviour of 1,2-dichloroethane and 1,2-dibromoethane: 1H-NMR, IR, refractive index and theoretical studies. *Phys. Chem. Liq.* **2006**, *44*, 315−328.

https://doi.org/10.1021/acsphyschemau.2c00055
ACS Phys. Chem Au 2023, 3, 157−166